How reliable are tephra layers as records of past eruptions? A calibration exercise

Cutler, N.A.[1]; Streeter, R.T.[2], Engwell, S.L.[3], Bolton, M.S.[4], Jensen, B.J.L.[4], Dugmore, A.J. [5, 6, 7]

[1] School of Geography, Politics & Sociology, Newcastle University, UK

[2] School of Geography & Sustainable Development, University of St Andrews, UK

[3] British Geological Survey, The Lyell Centre, Research Avenue South, Edinburgh EH14 4AP, UK

[4] Department of Earth and Atmospheric Sciences, University of Alberta, Edmonton, Alberta, Canada T6G 2E9

[5] School of Geosciences, University of Edinburgh, UK

[6] Department of Anthropology, Washington State University, USA

[7] Graduate Center, City University of New York, USA

Corresponding author:

Nick A Cutler, School of Geography, Politics & Sociology, 5th Floor Claremont Tower, Newcastle University, Newcastle upon Tyne, NE1 7RU, UK

Email: nick.cutler@ncl.ac.uk

Abstract

Tephra layers are frequently used to reconstruct past volcanic activity. Inferences made from tephra layers rely on the assumption that the preserved tephra layer is representative of the initial deposit. However, a great deal can happen to tephra after it is deposited; thus, tephra layer taphonomy is a crucial but poorly understood process. The overall goal of this research was to gain greater insight into the taphonomy of terrestrial tephra layers. We approached this by a) conducting a new survey of the tephra layer from the recent, well-studied eruption of Mount St Helens on May 18th, 1980 (MSH1980); b) modelling the tephra layer thickness using an objective mathematical technique and c) comparing our results with an equivalent model based on measurements taken immediately after the eruption. In this way, we aimed to quantify any losses and transformations that have occurred. During our study, we collected measurements of tephra layer thickness from 86 locations ranging from < 20 to > 600 km from the vent. Geochemical analysis was used to verify the identity of tephra of uncertain origin. Our results indicated that the extant tephra layer at undisturbed sites was representative of the original deposit: overall, preservation in these locations (in terms of thickness, stratigraphy and geochemistry) had been remarkably good. However, isopach maps generated from our measurements diverged from isopachs derived from the original survey data. Furthermore, our estimate of the quantity of tephra produced during eruption greatly exceeded previous estimates of the fallout volume. In this case, inaccuracies in the modelled fallout arose from issues of sampling strategy, rather than taphonomy. Our results demonstrate the sensitivity of volcanological reconstructions to measurement location, and the great importance of reliably measured low/zero values in reconstructing tephra deposits.

Keywords: Mount St Helens; volcanological reconstruction; isopach maps; cubic B-spline; taphonomy; electron microprobe

1. Introduction

Tephra layers are frequently used to reconstruct records of past volcanic activity, and to infer the characteristics of the eruptions that produced them (Bonadonna and Houghton, 2005; Carey and Sparks, 1986; Pyle, 1989). This research is necessary to expand the short and rather patchy record of volcanic eruptions based on historical accounts, and is fundamental to understanding volcanic processes (Bonadonna et al., 2015; Bonadonna et al., 1998; Carey and Sparks, 1986). However, inferences made from tephra layers rely on the assumption that the preserved tephra layer is representative of the initial deposit. A great deal can happen to tephra after deposition (e.g., Dugmore et al., in press), and recent research has demonstrated that environmental conditions (notably vegetation cover) play a key role in determining how much of the deposit is preserved *in situ* (Blong et al., 2017; Cutler et al., 2016a; Cutler et al., 2016b; Dugmore et al., 2018). In terrestrial settings, tephra deposits can be re-worked by the elements and slope processes, sometimes for a period of years (e.g., Liu et al., 2014; Panebianco et al., 2017; Wilson et al., 2011). Once interred, tephra layers may be altered by bioturbation, soil processes (e.g., eluviation) and geochemical transformation. Thus, even apparently well-preserved tephra layers may not record the characteristics of the fresh deposit faithfully: taphonomy matters. Despite the implications for volcanogenic reconstruction, the ways that tephra deposits are preserved (or not) are poorly understood. Our research targets this knowledge gap, aiming to gain greater insight into the taphonomy of terrestrial tephra layers, and, by extension, an improved understanding of past volcanism.

Our strategy was to survey a buried tephra layer produced by a recent, well-studied eruption, and to compare our data with measurements taken soon after deposition, thereby calibrating any losses and transformations that occurred during the nearly 40-year intervening period. We focussed our study on the tephra layer produced by the May 18th 1980 eruption of Mount St Helens (hereafter, MSH1980). The MSH1980 tephra layer was particularly suited to a study of this type because the US Geological Survey (USGS) measured it within 2-3 days of the eruption, before it had been substantially reworked (Sarna-Wojcicki et al., 1981). The 1980 survey of the fresh deposit collected over 200 measurements of tephra thickness, extending more than 600 km from the vent (Sarna-Wojcicki et al., 1981). This rich dataset gives an unparalleled record of baseline conditions, and facilitates the production of detailed isopach maps and volume estimates (Engwell et al., 2015).

We conducted an initial survey of the MSH1980 layer in 2015 (Cutler et al., 2018). We found that the preservation of the layer was remarkably good in certain settings. The overall characteristics of the original deposit were retained in the tephra layer (i.e., systematic thinning along and across the main plume axis and a marked secondary thickening ~300 km

from the vent). Grain size characteristics of the initial deposit (originally established by Carey and Sigurdsson, 1982; Durant et al., 2009; Eychenne et al., 2015) were also preserved. However, our initial samples were concentrated in two areas, one proximal (20-40 km) and one distal (~300 km) to Mount St Helens. We therefore conducted further field measurements in 2018, aiming to extend the range and density of our sampling. In particular, we wanted to collect more data from a) areas towards the edge of the tephra deposit b) points along the tephra deposit's main axis, and c) areas under-sampled in the original (1980) survey. Our objective was to construct isopach maps of the MSH1980 layer using an objective statistical model (Engwell et al., 2015), and to compare this isopach map with a similar map produced from the 1980 survey data.

Constructing isopach maps from terrestrial tephra layers is a standard procedure in volcanology (Cioni et al., 2015; Engwell et al., 2015; Klawonn et al., 2014a; Klawonn et al., 2014b). The key difference with our project is that we constructed isopachs from both the original (1980) measurements, and the extant tephra layer, using the same methodology. This allowed us to objectively compare the 'before-and-after' isopach maps, and identify variability in preservation, and quantify how well a tephra layer can represent the fresh fallout. We anticipated that a reconstruction of the fallout based on the extant tephra layer would substantially underestimate the volume of tephra produced, due to the winnowing of fine material and the erosion/compaction of thin deposits on the margins of the fallout zone.

2. Methods

2.1 Sampling strategy

In 2015, we measured the thickness of the MSH1980 layer in two areas: the Gifford Pinchot National Forest (GPNF), 20-40 km from Mount St Helens and around Ritzville (approximately 300 km from the vent). Details of the survey are available in Cutler et al. (2018). To fill gaps in our 2015 survey, we supplemented these points with locations on the eastern margins of the Cascades (the eastern part of the GPNF and the southern Wenatchee National Forest/White Pass area); in central Washington State; and in locations beyond Ritzville (extending eastwards into Idaho and Montana) (Fig. 1). Our sampling locations encompassed two distinctive vegetation types: coniferous forest in the west, and sparse, shrubby vegetation (known as sagebrush steppe) in the arid east of the survey area.

Many of our sampling locations were in intensively managed agricultural areas. The tephra that fell in this region in 1980 was relatively thin (typically 5-30 mm; Fig. 1) and vulnerable to disturbance by agricultural activities. Consequently, our 2018 fieldwork in central Washington

State focussed on areas set aside for nature conservation, as we reasoned that a) levels of surface disturbance would be lower than the surrounding farmland and b) the management regimes of the past forty years or so would be well documented. Tephra deposits are reworked by wind and rain; where the deposits are thin, it may be lost entirely. Consequently, we concentrated on areas that received > 5 mm (uncompacted) thickness of tephra in 1980, to increase the chance of finding the MSH1980 layer. We did not core lakes or sample wetland habitats.

At each site, we selected locally flat sampling locations in areas that we judged suitable for preservation (e.g., with mature, undisturbed vegetation). Summer wildfires are common occurrences in Washington State, and intense burns are associated with a loss of soil stability and increased geomorphological activity that could easily disturb tephra deposits and layers. We therefore avoided sampling locations that had been obviously disturbed by fire. We also avoided areas of obvious bioturbation, e.g., ground trampled by large herbivores or disrupted by burrows.

[Fig. 1]

2.2 Tephra measurements

Measurements of the tephra layer were collected by two teams (Appendix A). Potential sampling locations were investigated with test pits; if the MSH1980 tephra layer was not located after opening ~10 pits, another sampling location was selected. Where the layer was present, a shallow soil section was opened up, and the thickness of the layer was measured. Team 1 (designated 'NAC' in Appendix A, Table A.1) opened three to nine sections (depending upon local tephra layer variability) in each sampling location, we recorded the representative thickness of the layer in each section, and calculated mean values. Team 2 generally made a single measurement of tephra thickness, although multiple pits were excavated at most sites. Both teams recorded stratigraphy where they observed clear stratigraphic units. A sediment sample was collected when the provenance of the tephra was uncertain.

2.3 Geochemical methodology

In locations close to the eruption source or main plume axis, the MSH1980 layer was relatively thick, and lay just below the soil surface (Cutler et al., 2018). As such, it was easy to identify based on stratigraphy and physical characteristics (presence of pumice grains, colour, grain size, etc.) In other, mainly distal, locations, the origin of tephra layers was harder to determine, and we used geochemical analyses to aid identification. A total of 20 tephra samples were processed and analysed at the University of Alberta. Samples rich in

organics were hand-picked or sieved to remove organic material larger than ~2 mm, then treated with 30% hydrogen peroxide solution for a minimum of 12 hours. All samples were sieved to consolidate material 150-75 μm in diameter. Glass from this fraction was extracted by density separation with lithium heteropolytungstate (LST) solution at 2.45 g cm^{-3}. Glass was analysed on a JEOL 8900 Superprobe using 15 KeV, 6 nA current and 5 μm beam. We used a small beam size because the MSH1980 tephra is vesicular and microlitic/phenocryst-rich (Eychenne et al., 2015). We took care to analyse clean glass; any analyses that demonstrated mineral contamination were withheld from comparison. To correct for Na-loss during analysis, time-dependent intensity correction was employed using Probe for EPMA software (Donovan et al., 2015). Analyses of secondary standards, a Lipari obsidian (ID 3506) and Old Crow tephra (UA 1099), were performed throughout analytical runs (e.g., Jensen et al., 2019; Kuehn et al., 2011) to evaluate calibration and to detect possible analytical complications. Sample glass geochemistries were compared to reference data from proximal samples from MSH and other Cascade volcanoes (Zhen-Hui et al., in press). Samples inconsistent with MSH1980 (blast/Plinian fall) and those that presented obviously mixed tephras (e.g., MSH1980 shards in addition to one or more substantial secondary populations from other sources) were excluded from the thickness modelling exercise.

2.4 Modelling of tephra thickness

We applied a mathematical model – cubic B-spline interpolation – to interpret the tephra thickness data. We produced two models from our 2015/18 survey data, one (Layer Model 1) based purely on our measurements, and one (Layer Model 2) that supplemented our data with 55 zero measurements from Durant et al. (2009) (Appendix A). We then compared these models with Engwell et al.'s (2015) analysis of the USGS survey data (hereafter, the Deposit Model). The results of cubic B-spline interpolation can be envisaged in terms of the deformation of a thin, elastic 'plate' under tension, where the plate represents the surface of the tephra deposit. Full details of the technique are given in Engwell et al. (2015). Briefly, we produced the Layer Models by fitting cubic B-splines using a modified version of the FORTRAN code of Inoue (1986). The method requires four fitting parameters, namely tension (τ), roughness (ρ), the grid size of the domain and measurement weightings (w_ρ). The parameters are set to produce a compromise between goodness-of-fit and excessive local distortion. Replicating the analysis of Engwell et al. (2015), we divided the area to be modelled into a 10 km grid, set w_ρ to 1 (i.e., all points weighted equally and with maximum weighting) and tension to a conventional value of 0.99 (Bauer et al., 1998; Inoue, 1986). We then varied the roughness parameter, which controls the balance between fit and overall surface roughness. Roughness values typically vary between 0.1 and 1000; small values give a very smooth fit and are sufficient where there is little local variation in data; larger values are required where the data are more variable. The fitted results are in the form of a

gridded dataset of interpolated thickness values across a specified x-y domain. We contoured the gridded data to produce isopach maps, assessing the isopachs from our 2015/18 survey on the basis of goodness of fit and visual credibility. The results were processed using GMT software (Wessel and Smith, 1991) to produce isopach maps with the same intervals used in Engwell et al's (2015) analysis (thinnest isopach = 0.1 mm in all cases). The volume of the modelled deposit was calculated by direct integration of the spline-derived surface within the 0.1 mm isopach.

3. Results

3.1 Tephra layer survey

We sampled tephra thickness in 27 locations in 2015; in 2018 we added a further 59 data points, giving 86 sampling locations in total (Fig. 2, Appendix A). Our samples were distributed over a wide area. The most distal location we sampled was just north of Missoula, MT, approx. 600 km from Mount St Helens. The most proximal location was east of Cougar, WA, about 13 km from the vent. Our dataset gave us good coverage of the sector of Washington State that received >5 mm of tephra in 1980, as well as some areas that received thinner deposits.

[Fig. 2]

Although many of our sampling locations had conditions conducive to the retention of tephra, they had still been exposed to processes that can disrupt thin deposits. For example, conservation management regimes in the wildlife reserves we visited included thinning of ponderosa pine stands and prescribed burning. Bioturbation was also frequent on many of our sites. In some locations, large herbivores (cattle and/or elk) had churned the soil to a depth of several centimetres; congregations of these animals - e.g., around feeding stations – had completely obliterated the tephra layer. Complexes of small burrows disrupted the deposit in areas where the soil was more than ~10 cm deep. Consequently, many of our sampling locations in eastern WA had thin, rocky soils or unbroken biocrust cover.

Although the MSH1980 layer was frequently discontinuous at a scale of a few metres to tens of metres, we found patches of tephra on most of the sites investigated, usually just below the surface (Fig. 3). The layer was largely absent in sampling locations where the initial deposit would have been less than ~5 mm thick in 1980. In the eastern part of our survey area, we often found the tephra beneath clumps of mature sagebrush, especially where the soil was too thin for burrowing animals, and a biocrust had stabilised the surface of the soil.

Further west, in areas of coniferous forest, the tephra was protected by a layer of forest duff (primarily pine needles), and often retained the stratigraphy first described by Waitt and Dzurisin (1981) (Fig. 3). Previous studies of Mount St Helens' tephra preservation indicate increased accumulation in forested, topographically concave microsites, relative to those that are open and convex (Collins and Dunne, 1986; Zobel and Antos, 1991).

[Fig. 3]

The tephra layer that we found closely approximated the thickness of the original deposit (compare our measurements with the isopachs generated from the 1980 survey: Fig. 2). This was particularly evident in a comparison of thickness measurements taken along the main axis of the eruption plume (Fig. 4). Both key features of the original deposit – a decay in thickness with distance, and a secondary thickening starting around 300 km from the vent – were captured by our measurements. We also observed thinning as we moved away from the main plume axis. For example, in the Quincy Lakes region, the tephra layer thinned from ~2 cm on the axis, to 1 cm 20 km to the north, eventually disappearing 25 km from the axis (~120° W on Fig. 2c). Intra-site variability was generally low (Fig. 4).

[Fig. 4]

3.2 Geochemical analysis

Twelve of the tephra samples analysed contained abundant glass that corresponded to the geochemistry of the MSH1980 reference samples (Appendix A; see also Zhen-Hui et al., in press). The remaining samples appeared to be MSH1980 tephra when observed *in situ*. However, geochemical analysis demonstrated they were either from older Mount St Helens eruptions (e.g., Layer T, A.D. 1800, UA 3177 and 3178) or were formed from mixtures of detrital glass from various Cascade Range eruptions (e.g., Mazama, Glacier Peak, and MSH). These samples were excluded from the tephra layer models.

We used our geochemical analysis to distinguish between glass produced during the Plinian phase of the eruption, and microlite-dense, 'cryptodome' material ejected during the lateral blast that preceded the Plinian phase. Blast material is most easily differentiated based on silica composition (Fig. 5) and morphology. Plinian glass chiefly exhibits silica values less than 76% by weight, with most shards registering 71-73% silica. Blast material contains substantially more silica (76-79% silica by weight, i.e., more evolved) (see Zhen-Hui et al., in press, for further details). Most of the MSH1980 samples were primarily comprised of glass from the Plinian phase. However, blast material was present in all samples, even into the distal plume. One sample, UA 3180, was entirely composed of blast material (Fig. 5). This

site was directly northeast of the vent and near the deposit's northern limit. The absence of Plinian glass here demonstrated that there is a near-vent region where appreciable Plinian fallout did not occur, though a visible unit was still deposited. The proportion of Plinian to blast material was not quantified. However, samples from the north of the proximal deposit appeared to be enriched with the latter, consistent with the findings of Eychenne et al. (2015). Further, although we confirmed the presence of the MSH1980 tephra in deposits, no attempt was made to evaluate the composition of samples in terms of glass vs non-tephra sediments.

[Fig. 5]

3.3 Isopach reconstruction and volume estimate

We struggled to produce realistic isopach maps from just our 2015/18 survey data (Layer Model 1). Specifically, it was difficult to get the thinner isopachs to close, due to the lack of data points from thin layers. We selected a roughness value of 100, to accommodate local variability in thickness values. Layer Model 1 captured the large-scale features of the tephra deposit, notably the thicker values around the vent, and the secondary thickening ~300 km from Mount St Helens. However, it diverged from the Deposit Model in several respects (Fig. 6b, c). Firstly, there were anomalous 'islands' of thickening in peripheral locations (Fig. 6b). Secondly, the zone of maximum thickness was offset to the west of the vent (labelled **A** in Fig. 6c). Thirdly, the 5 mm and 10 mm isopachs were much more extensive in Layer Model 1, leading to higher estimated thicknesses (red tones, e.g., **B** in Fig. 6c) in distal regions of the fallout. Regions where Layer Model 1 produced lower values than the Deposit Model (blue tones) were more restricted. This was reflected in the volume estimates. The volume estimate - calculated as the area under the surface within the 0.1 mm isopach - for Layer Model 1 was 320% larger than that from the Deposit Model (Table 1).

Layer Model 2, which included zero values from Durant et al. (2009), was a closer match to the Deposit Model. We selected a roughness value of 100, to facilitate comparison with Layer Model 1. In addition to replicating most of the large-scale features of the original deposit, the thinner isopachs closed more readily, eliminating most of the anomalous peripheral zones (Fig. 6d). The zone of thickening around the vent tallied with contemporary observations, as did the north-south extent of the zone receiving tephra. Differences between Layer Model 2 and the Deposit Model were generally ±1 mm (yellow and pale blue shading in Fig. 6d). There were some exceptions, notably two distal regions where the interpolated values in Layer Model 2 were >30 mm greater than the Deposit Model (labelled **C** and **D** in Fig. 6e). The volume estimate for Layer Model 2 was about 66% greater than the Deposit Model estimate (Table 1).

[Fig. 6]

[Table 1]

4. Discussion

The MSH1980 tephra layer has retained many of the features noted when the deposit was originally mapped in the days after the eruption. Despite numerous sources of potential disruption, the preserved thicknesses we measured closely approximated the values recorded in 1980. However, reconstructions of the tephra fallout based on the extant tephra layer (Layer Models) are markedly different from a model based on contemporary measurements, both in terms of the distribution of the tephra, and its estimated volume. Unexpectedly, the Layer Models substantially *overestimated* the volume of the deposit, even though thin deposits were undoubtedly lost to erosion. Our results demonstrate the importance of sampling strategy and taphonomy, when developing eruption volume estimates.

4.1 Tephra preservation

We found very little evidence for the large-scale mobilisation of the MSH1980 tephra deposit in the immediate aftermath of the eruption. The mobilisation of fresh tephra deposits leads to losses (thinning) in some areas, and gains (over-thickening) in others (Dugmore et al., 2018). Our samples covered area of several thousand km^2, spanning two very different vegetation types and a wide range of initial thicknesses (~5 – 100 mm); where the layer survived, we observed consistently good preservation, in terms of thickness, stratigraphy and geochemistry. However, it is important to note that varying depositional environments and differences in vegetation cover may produce marked differences in preservation potential, especially for thin deposits (Blong et al., 2017). Further, as observed by Blong et al. (2017), even when environmental conditions are held more-or-less constant (e.g., deposition under forest cover) preservation/erosion regimes may differ meaningfully.

We observed some instances of over-thickening in our 2015 survey (Cutler et al., 2018), but this phenomenon was restricted to a handful of proximal sites. Furthermore, our previous study indicated that the MSH1980 tephra contains very low levels of organic matter (i.e., the layer had not been 'bulked up' by post-depositional additions of material: Cutler et al., 2018). It is possible that mixing with matrix sediment could have increased the thickness of the tephra layer (Ver Straeten, 2008). One would expect this to be particularly significant on arid, distal sites in eastern Washington State, where primary productivity is lower than the west,

and the soils have a high proportion of loess. However, the sharpness of the top and bottom contacts of the tephra layer in many distal locations suggests that this effect is limited.

Based on our observations, the factors that facilitated preservation in the sedimentary record appeared to be a) limited anthropogenic disturbance; b) conditions that limited bioturbation by large herbivores and burrowing animals (e.g., woody plant cover, thin soils) and c) biogenic surface cover (dense vegetation, litter or biocrust) that acted to stabilize tephra shortly after deposition. Field observations suggested that low-intensity wildfires in the sagebrush steppe left the moss/lichen biocrust (and, by extension, the underlying tephra layer) largely untouched. In areas where fire damage consumed the woody vegetation and damaged the underlying biocrust the tephra layer was often absent.

Unsurprisingly, the MSH1980 tephra layer became harder to find on the margins of the fallout zone. The geochemical analysis also demonstrated that it became harder to identify reliably in the field. Our survey suggested that formation of a distinct tephra layer visible to the naked eye was unlikely in areas that received less than ~5-8 mm of tephra in 1980. This applied to areas where the preservation potential was good (e.g., nature reserves in eastern WA where biocrust cover was extensive). This figure matches the proposed threshold of 'geological preservation' for tephra of ~5 mm (Pyle, 2016; Sparks et al., 1983). It places an upper limit on the accuracy of fallout reconstruction from terrestrial sites, especially where a high proportion of the tephra is deposited in thin layers. This has important ramifications for distal-inclusive volume estimates, especially for ancient eruptions, wherein deposits dominated by low Reynolds number particles are less likely to be preserved (Bonadonna et al., 1998).

Our survey was not exhaustive and improvements are possible in terms of a) the distribution of sampling locations and b) the range of land cover types sampled. In terms of the distribution of our sampling locations, we collected few samples from the zone < 20 km from Mount St Helens. Large parts of this zone were profoundly affected by the initial blast, and subsequent catastrophic events (lahars and pyroclastic flows). Although good Plinian fall deposits exist in this zone, the post-eruption extirpation of vegetation, combined with steep topography, make them harder to find and interpret. Collins and Dunne (1986) noted the near-vent region incurred substantial degradation, of 10-100+ mm in the first months to years following the eruption, depending on topography. We and the researchers who surveyed the fresh tephra deposit did not make measurements in the zone immediately around the volcano (Sarna-Wojcicki et al., 1981). Our survey only encompassed a narrow range of land types, mainly areas of mature vegetation in nature reserves. Furthermore, we did not collect samples from lakes or wetlands, where preservation (both of primary and remobilised deposits) might have been better. Future sampling might investigate aquatic environments.

These settings might have different, thinner, preservation thresholds, although there will also be different taphonomic issues to contend with. We also preferentially sampled sites we considered optimal for preservation. Had we sampled the fallout area randomly or systematically, many measurements would likely have been null values. However, we suspect that our approach to filtering sampling locations is not unusual, i.e., other researchers are likely to establish criteria for site selection that maximise their chances of encountering representative tephra layers.

The MSH1980 layer is relatively young and close to the surface. Although it closely resembles the initial deposit, it may yet be transformed further by physical processes (e.g., compaction, bioturbation, eluviation) or chemical weathering. Further research will be required to establish the impact of ageing on tephra layer preservation. However, our results demonstrate that terrestrial tephra deposits can faithfully preserve the characteristics of fresh tephra deposits under a range of conditions. Indeed, where preservation is good and post-depositional remobilisation is limited, establishing the maximum thickness of the tephra layer is probably provides a good approximation of initial deposit thickness.

4.2 Modelling the fallout

The tephra layer in our sampling locations closely approximated the thickness of the initial deposit (Klawonn et al., 2014b). However, the reconstructions of the fallout based on our measurements differed substantially from the equivalent model based on the 1980 USGS survey. Furthermore, the estimated bulk volume *exceeded* the value from the Deposit Model, when we anticipated a loss of material from the tephra layer due to erosion. Our sampling effort (in terms of the number of measurements taken) was similar to, or higher than, previous studies that have reconstructed eruption volume from tephra layers (S. Engwell, unpublished data and Alfano et al., 2011; Biass and Bonadonna, 2011; Bursik et al., 1992; Nathenson, 2017; Yang and Bursik, 2016). Our points were also distributed over a wide area, encompassing both proximal and distal locations. The reason Layer Model 1 performed poorly was probably not taphonomy, but the spatial distribution of sample locations, specifically a) a lack of low/zero thickness measurements in peripheral and near-vent locations and b) an uneven distribution of sample locations within the main fallout zone.

Layer Model 1 could not model isopachs thinner than 5 mm realistically, due to a sparsity of low and zero values on the margins of the fallout zone. Without these constraining points, anomalous values appeared far from the areas we measured and the area of thicker isopachs increased, inflating the volume estimates. The value of constraining measurements was demonstrated by the inclusion of zero values in Layer Model 2, which resulted in a more plausible estimate of tephra distribution and volume. Layer Model 2 indicated that collecting

further measurements around the periphery of the fallout zone would have eliminated anomalous high values in Layer Model 1 (e.g., to the west of Mount St Helens, or in the lobe centred on 118°W, 46.5°N: labelled **A** and **B**, respectively, on Fig. 6c), thereby reducing the estimated volume of tephra.

The spatial distribution of sampling locations was also important. We focussed on accessible areas where we thought that preservation was likely to be good. This led to an inevitable clustering of samples, and extensive, under-sampled locations. The unevenness of our sampling probably resulted in the large divergences between the Deposit and Layer Models. For example, there were no sampling locations to the north of our sites around Ritzville (mean tephra thickness ~40 mm); when zero values were added in Layer Model 2, the model had to accommodate a north-south gradient of 40 to 0 mm, resulting in an anomalously thick zone (labelled **C** in Fig. 6e).

When reconstructing a tephra deposit, it is desirable to have numerous, evenly distributed sampling locations that span the whole fallout zone. Unfortunately, this is rarely achievable. Including peripheral locations greatly increases the area that has to be surveyed, and locating thin, easily disrupted tephra layers is necessarily time-consuming. If there is a geological limit to tephra layer preservation in terrestrial sites, then modelling isopachs thinner than this limit will always be challenging. Furthermore, ensuring an even distribution of samples (similar to the transects established by the USGS in 1980) may not be possible, especially in inaccessible locations, or where preservation varies greatly from place-to-place. When the extent of the plume is not known (typical of long-past eruptions), it is tempting to concentrate on areas where tephra is found. However, our study powerfully reinforces the value of reliably established ('true') zero measurements when it comes to modelling tephra deposits and, by extension, eruption dynamics.

5. Conclusions

The thickness of the MSH1980 tephra layer measured in 2015-18 was representative of the initial deposit. Indeed, preservation was remarkably good in areas where the fresh deposit appears to have been interred/sealed shortly after the eruption. However, the reconstruction of the MSH1980 fallout based on our measurements only captured the largest scale features of the deposit. There was considerable variance in detail, especially in areas where the thickness varied markedly over short distances. Furthermore, our reconstructions overestimated the volume of fallout, despite the inclusion of dozens of measurements distributed over a large portion of the fallout zone. Our model improved markedly when we added constraining (zero) values from marginal locations. Our findings have implications for

others seeking to reconstruct long-past volcanic eruptions from terrestrial tephra layers. Specifically, they highlight the importance of sampling strategy in the reconstruction of tephra deposits: even with excellent preservation conditions and many measurements, it is still possible for estimates to vary markedly from the true value.

Acknowledgements

We are grateful to the Washington Department of Fish and Wildlife and the site managers of the Revere, Seep Lakes, Goose Lakes, Lower Crab Creek, Quincy Lakes, Whiskey Dick, L.T. Murray and Oak Creek Wildlife Areas for granting access to field sites. We are also grateful to the US Fish and Wildlife Service and the site manager of the Turnbull National Wildlife Reserve for permitting us to conduct our surveys.

Funding

This research was supported by grants from the Royal Geographical Society (ref: SRG 01/18) and Quaternary Research Association to NAC.

References

Alfano, F., Bonadonna, C., Volentik, A.C.M., Connor, C.B., Watt, S.F.L., Pyle, D.M. and Connor, L.J., 2011. Tephra stratigraphy and eruptive volume of the May, 2008, Chaitén eruption, Chile. B Volcanol, 73(5): 613-630.

Bauer, S., Swenson, M.S., Griffa, A., Mariano, A.J. and Owens, K., 1998. Eddy mean flow decomposition and eddy-diffusivity estimates in the tropical Pacific Ocean 1. Methodology. Journal of Geophysical Research-Oceans, 103(C13): 30855-30871.

Biass, S. and Bonadonna, C., 2011. A quantitative uncertainty assessment of eruptive parameters derived from tephra deposits: the example of two large eruptions of Cotopaxi volcano, Ecuador. B Volcanol, 73(1): 73-90.

Blong, R., Enright, N. and Grasso, P., 2017. Preservation of thin tephra, Journal of Applied Volcanology.

Bonadonna, C., Biass, S. and Costa, A., 2015. Physical characterization of explosive volcanic eruptions based on tephra deposits: Propagation of uncertainties and sensitivity analysis. Journal of Volcanology and Geothermal Research, 296: 80-100.

Bonadonna, C., Ernst, G.G.J. and Sparks, R.S.J., 1998. Thickness variations and volume estimates of tephra fall deposits: the importance of particle Reynolds number. Journal of Volcanology and Geothermal Research, 81(3-4): 173-187.

Bonadonna, C. and Houghton, B.F., 2005. Total grain-size distribution and volume of tephra-fall deposits. B Volcanol, 67(5): 441-456.

Bursik, M.I., Sparks, R.S.J., Gilbert, J.S. and Carey, S.N., 1992. Sedimentation of tephra by volcanic plumes: 1. Theory and its coparison with a study of the Fogo A plinian deposit, Sao Miguel (Azores). B Volcanol, 54(4): 329-344.

Carey, S. and Sparks, R.S.J., 1986. Quantitative models of the fallout and dispersal of tephra from volcanic eruption columns. B Volcanol, 48(2): 109-125.

Carey, S.N. and Sigurdsson, H., 1982. Influence of particle aggregation on deposition of distal tephra from the May 18, 1980, eruption of Mount St. Helens volcano. Journal of Geophysical Research, 87: 7061-7072.

Cioni, R., Pistolesi, M. and Rosi, M., 2015. Plinian and subplinian eruptions. In: H. Sigurdsson, S. McNutt, H. Rymer, J. Stix and B. Houghton (Editors), Encyclopedia of Volcanoes. Elsevier Science & Technology, London, pp. 520-536.

Collins, B.D. and Dunne, T., 1986. Erosion of the tephra from the 1980 eruption of Mount St Helens. Geological Society of America Bulletin, 97(7): 896-905.

Cutler, N.A., Bailey, R.M., Hickson, K.T., Streeter, R.T. and Dugmore, A.J., 2016a. Vegetation structure influences the retention of airfall tephra in a sub-Arctic landscape. Prog Phys Geog, 40(5): 661-675.

Cutler, N.A., Shears, O.M., Streeter, R.T. and Dugmore, A.J., 2016b. Impact of small-scale vegetation structure on tephra layer preservation, Sci Rep-UK.

Cutler, N.A., Streeter, R.T., Marple, J., Shotter, L.R. and Dugmore, A.J., 2018. Tephra transformations: variable preservation of tephra layers from two well-studied eruptions, B Volcanol.

Donovan, J.J., Kremser, D., Fournelle, J.H. and Goemann, K., 2015. Probe for EPMA. Probe Software, Eugene, OR.

Dugmore, A., Streeter, R. and Cutler, N., 2018. The role of vegetation cover and slope angle in tephra layer preservation and implications for Quaternary tephrostratigraphy. Palaeogeogr Palaeocl, 489: 105-116.

Dugmore, A.J., Thompson, P.I.J., Streeter, R.T., Cutler, N.A., Kirkbride, M.P. and Newton, A.J., in press. The interpretative value of transformed tephra sequences. Journal of Quaternary Science.

Durant, A.J., Rose, W.I., Sarna-Wojcicki, A.M., Carey, S. and Volentik, A.C.M., 2009. Hydrometer-enhanced tephra sedimentation: constraints from the 18 May eruption of Mount St Helens, Journal of Geophysical Research.

Engwell, S.L., Aspinall, W.P. and Sparks, R.S.J., 2015. An objective method for the production of isopach maps and implications for the estimation of tephra deposit volumes and their uncertainties, B Volcanol.

Eychenne, J., Cashman, K., Rust, A. and Durant, A., 2015. Impact of the lateral blast on the spatial pattern and grain size characteristics of the 18 May 1980 Mount St. Helens fallout deposit. Journal of Geophysical Research-Solid Earth, 120(9): 6018-6038.

Inoue, H., 1986. A least-squares smooth fitting for irregularly spaced data: finite-element approach using the cubic B-spine basis. Geophysics, 51(11): 2051-2066.

Jensen, B.J.L., Beaudoin, A.B., Clynne, M.A., Harvey, J. and Vallance, J.W., 2019. A re-examination of the three most prominent Holocene tephra deposits in western Canada: Bridge River, Mount St. Helens Yn and Mazama. Quaternary International, 500: 83-95.

Klawonn, M., Houghton, B.F., Swanson, D.A., Fagents, S.A., Wessel, P. and Wolfe, C.J., 2014a. Constraining explosive volcanism: subjective choices during estimates of eruption magnitude. B Volcanol, 76(2).

Klawonn, M., Houghton, B.F., Swanson, D.A., Fagents, S.A., Wessel, P. and Wolfe, C.J., 2014b. From field data to volumes: constraining uncertainties in pyroclastic eruption parameters. B Volcanol, 76(7).

Kuehn, S.C., Froese, D.G. and Shane, P.A.R., 2011. The INTAV intercomparison of electron-beam microanalysis of glass by tephrochronology laboratories: results and recommendations. Quaternary International, 246: 19-47.

Liu, E.J., Cashman, K.V., Beckett, F.M., Witham, C.S., Leadbetter, S.J., Hort, M.C. and Guomundsson, S., 2014. Ash mists and brown snow: Remobilization of volcanic ash from recent Icelandic eruptions. Journal of Geophysical Research-Atmospheres, 119(15): 9463-9480.

Nathenson, M., 2017. Revised tephra volumes for Cascade Range volcanoes. Journal of Volcanology and Geothermal Research, 341: 42-52.

Panebianco, J.E., Mendez, M.J., Buschiazzo, D.E., Bran, D. and Gaitan, J.J., 2017. Dynamics of volcanic ash remobilisation by wind through the Patagonian steppe after the eruption of Cordon Caulle, 2011. Sci Rep-UK, 7.

Pyle, D.M., 1989. The thickness, volume and grainsize of tephra fall deposits. B Volcanol, 51(1): 1-15.

Pyle, D.M., 2016. Field observations of tephra fallout. In: S. Mackie, K. Cashman, H. Ricketts, A. Rust and M. Watson (Editors), Volcanic Ash. Elsevier, Amsterdam, pp. 25-38.

Sarna-Wojcicki, A.M., Shipley, S., Waitt, R.B., Dzurisin, D. and Wood, S.H., 1981. Areal distribution, thickness, mass, volume, and grain size of air-fall ash from the six major eruptions in 1980. In: P.W. Lipman and D.R. Mullineaux (Editors), The 1980 eruption of Mount St Helens, Washington, U.S. U.S. Department of the Interior, USGS, Washington D.C., pp. 577-600.

Sparks, R.S.J., Brazier, S., Huang, T.C. and Muerdter, D., 1983. Sedimentology of the Minoan deep-sea tephra layer in the Aegean and Eastern Mediterranean. Marine Geology, 54(1-2): 131-167.

Ver Straeten, C.A., 2008. Volcanic tephra bed formation and condensation processes: a review and examination from Devonian stratigraphic sequences. Journal of Geology, 116(6): 545-557.

Waitt, R.B. and Dzurisin, D., 1981. Proximal air-fall deposits from the May 18 eruption - stratigraphy and field sedimentology. In: P.W. Lipman and D.R. Mullineaux (Editors), The 1980 eruption of Mount St. Helens, Washington. US Department of the Interior, USGS, Washington D.C., pp. 601-616.

Wessel, P. and Smith, W.H.F., 1991. Free software helps map and display data. Eos, 72(441): 445-446.

Wilson, T.M., Cole, J.W., Stewart, C., Cronin, S.J. and Johnston, D.M., 2011. Ash storms: impacts of wind-remobilised volcanic ash on rural communities and agriculture following the 1991 Hudson eruption, southern Patagonia, Chile. B Volcanol, 73(3): 223-239.

Yang, Q.Y. and Bursik, M., 2016. A new interpolation method to model thickness, isopachs, extent, and volume of tephra fall deposits, B Volcanol.

Zhen-Hui, F., Jensen, B.J.L. and Bolton, M., in press. Glass geochemical compositions from widespread tephras erupted over the last ~200 years from Mount St. Helens. Journal of Quaternary Science

Zobel, D.B. and Antos, J.A., 1991. 1980 tephra from Mount St Helens - spatial and temporal variation beneath forest canopies. Biol Fert Soils, 12(1): 60-66.

Tables

Model	Comments	Estimated tephra volume (m^3 DRE)	Difference from fresh deposit
Deposit Model	Based on 1980 survey	5.0×10^8	-
Layer Model 1	Based on 2015/18 survey	1.6×10^9	+320%
Layer Model 2	2015/18 measurements + zero values from 1980 survey	8.3×10^8	+66%

Table 1: Estimated tephra volume, calculated as the volume under a surface derived using cubic B-spline interpolation and bounded by the 0.1 mm isopach (Engwell et al., 2015).

Figures

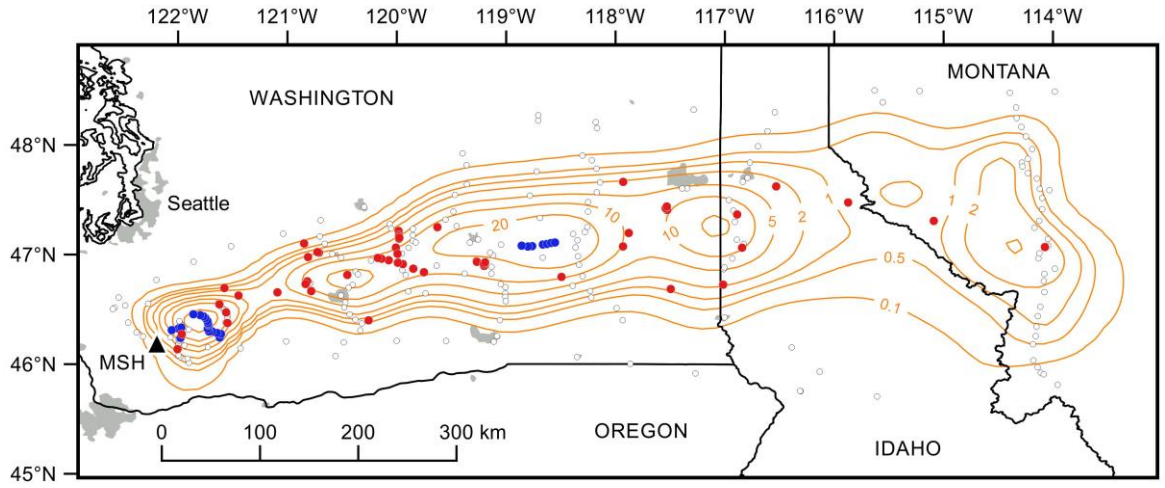

Fig. 1: Location plan. Sampling locations from the original (1980) USGS survey of the tephra deposit are indicated with open circles; our 2015 survey sites (Cutler et al., 2018) are indicated with blue circles; the 2018 survey locations are red. The orange lines are isopachs modelled by Engwell et al. (2015), using the 1980 survey data; tephra thickness is in mm.

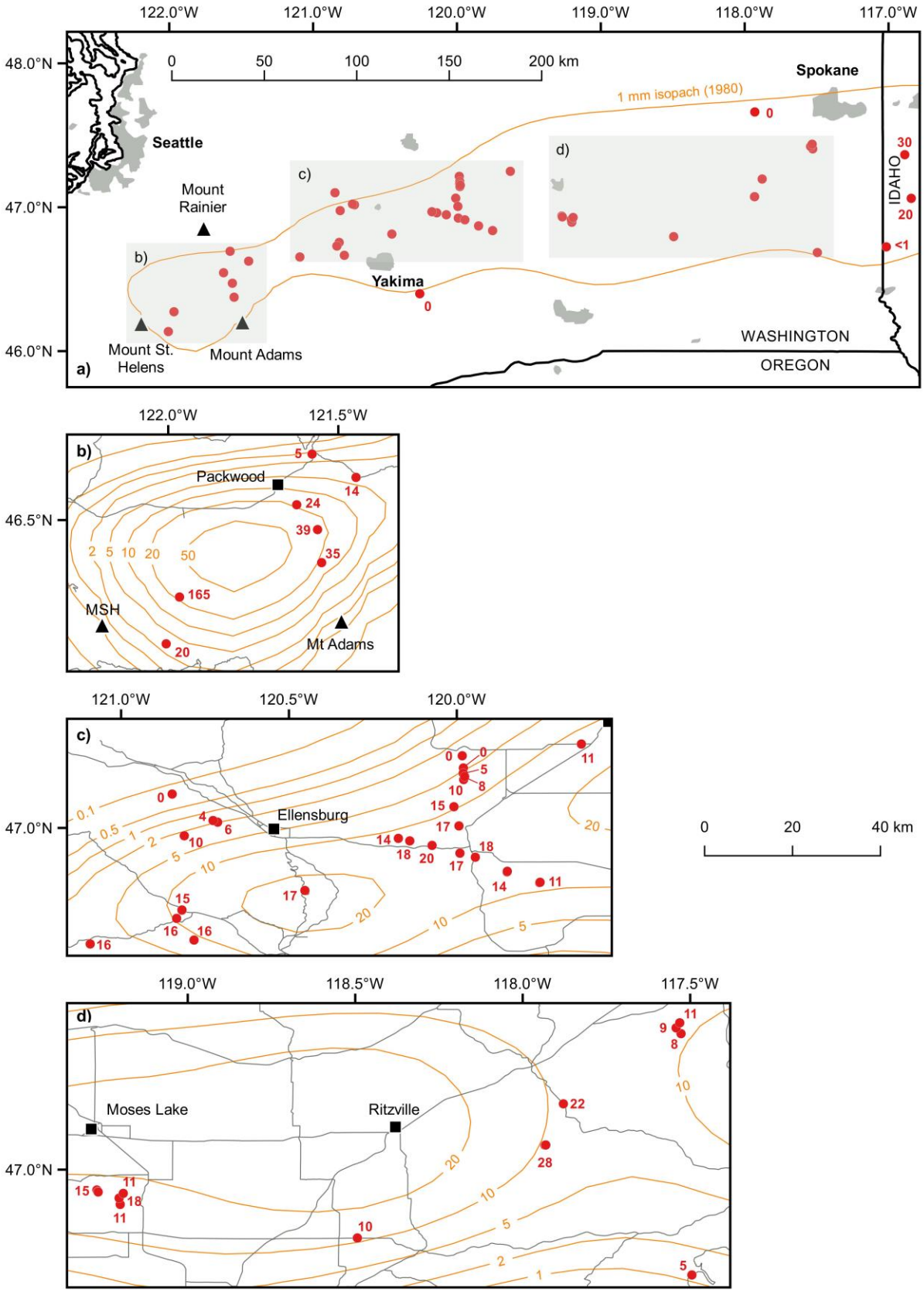

Fig. 2: MSH1980 thickness measurements from our 2018 survey (red points, with mean thickness in mm also in red). The orange isopach lines (with thickness in mm), shown for comparison, are from Engwell et al. (2015).

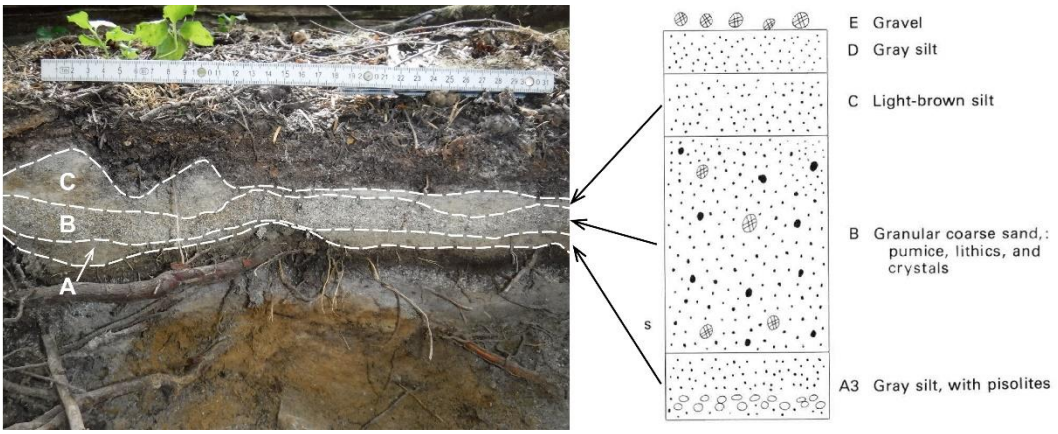

Fig. 3: A typical section from the GPNF (logged in 2018) compared with Waitt and Dzurisin's (1981) description of the fallout ~40 km from Mount St Helens; three of the units identified in 1980 (labelled A, B & C on the photograph) are clearly visible in the extant tephra layer. Note the older, pale grey tephra layer a few cm below MSH1980.

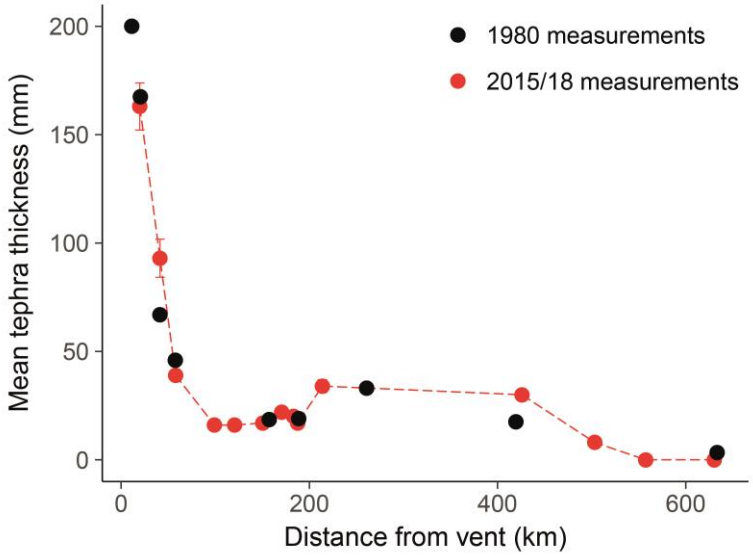

Fig. 4: A comparison of the extant MSH1980 tephra layer with measurements of tephra thickness made at the time of eruption. Original (1980) measurements are in black; mean thickness measured in 2015-2018 is shown in red; error bars indicate 1 SE. Measurements lie on or close to the main plume axis. Note the distinct secondary thickening between 200 and 400 km in both datasets.

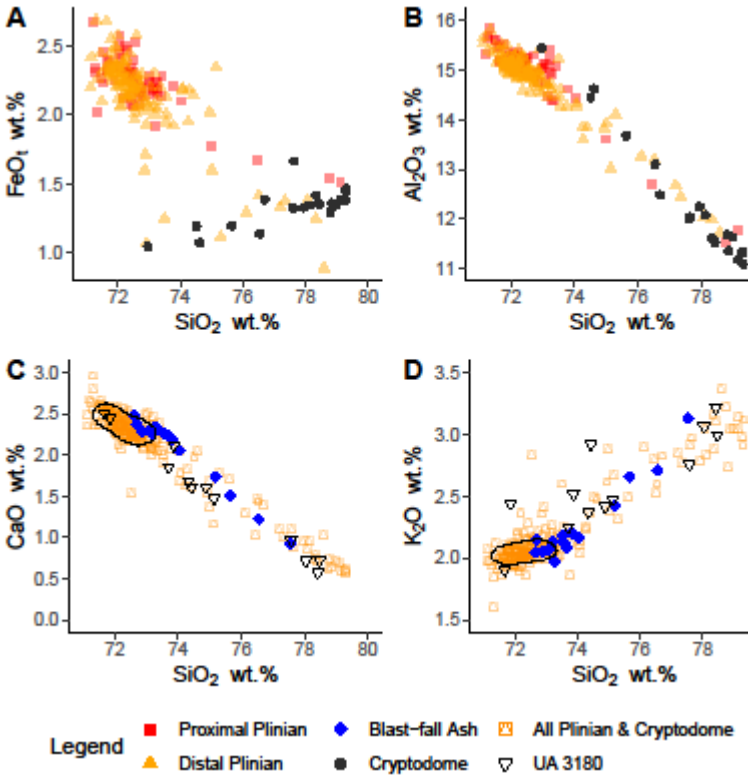

Fig. 5: Geochemical plots of MSH1980 glass demonstrating agreement between distal and proximal Plinian samples and relationship with cryptodome material and blast-fall ash. High-density regions for Plinian and cryptodome are highlighted (black contour = zone containing ~60% data; panels C and D). Note UA 3180 contains glass most similar to blast-fall ash but is unlike typical "Plinian" glass (C, D). FeOt = all Fe as FeO..

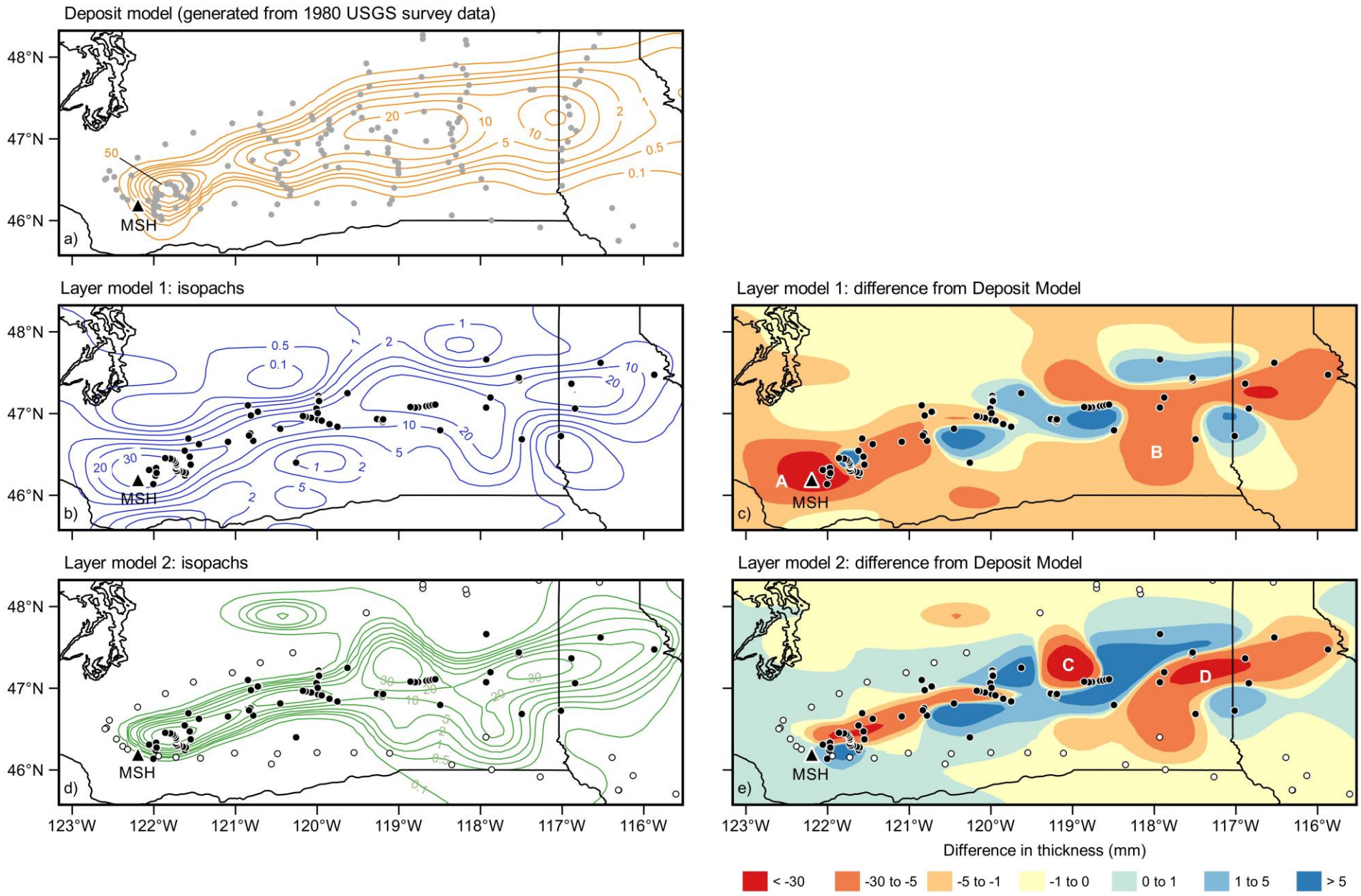
Deposit model (generated from 1980 USGS survey data)
Layer model 1: isopachs
Layer model 1: difference from Deposit Model
Layer model 2: isopachs
Layer model 2: difference from Deposit Model
MSH
a)
b)
c)
d)
e)
A
B
C
D
48°N
47°N
46°N
123°W
122°W
121°W
120°W
119°W
118°W
117°W
116°W
Difference in thickness (mm)
< -30
-30 to -5
-5 to -1
-1 to 0
0 to 1
1 to 5
> 5

Fig. 6: A comparison of isopach maps generated using the cubic B-spline approach of Engwell et al. (2015). Panel (a) shows the Deposit Model, an isopach map generated from the 1980 survey data, with the original survey locations indicated by grey circles. Panel (b) is an isopach map of our 2015/18 survey data (Layer Model 1), with our sampling locations indicated by black circles. Panel (c) compares the interpolated tephra thicknesses, and was generated by subtracting the output of Layer Model 1 from the Deposit Model; negative values (red tones) indicate that the thickness in the Layer Model exceeds that in the Deposit Model for a given location; negative values (blue tones) indicate the opposite. Panels (d) and (e) are isopach and difference maps, respectively, for Layer Model 2 (zero points from the 1980 USGS survey are indicated by open circles). A, B and C indicate regions where the Layer Model estimates greatly exceed the deposit model. All thickness values are in mm.

Appendix A

Site	Collector	Year	N	E	T (mm)	SE
WHI001	NAC	2018	46.94793	-120.07385	20	0.9
WHI002	NAC	2018	46.96144	-120.14027	18	0.6
WHI003	NAC	2018	46.96887	-120.17421	14	0.9
3*	NAC	2018	46.81373	-120.45265	17	2.1
LTM001	NAC	2018	46.97667	-120.81192	10	1.3
LTM002	NAC	2018	47.01706	-120.71250	4	0.5
LTM003	NAC	2018	47.02210	-120.72626	6	0.6
LTM004	NAC	2018	47.10091	-120.84796	0	0.0
OAK001	NAC	2018	46.66606	-120.78286	16	0.3
OAK002	NAC	2018	46.75462	-120.81903	15	1.2
OAK003	NAC	2018	46.75568	-120.81884	21	2.6
OAK004	NAC	2018	46.73061	-120.83476	16	1.8
PAC001	NAC	2018	46.37484	-121.54915	35	3.1
PAC002	NAC	2018	46.47197	-121.56113	39	1.9
PAC003-4	NAC	2018	46.54497	-121.62243	24	1.1
WP01	NAC	2018	46.62543	-121.44805	14	0.3
WP02	NAC	2018	46.65441	-121.09216	16	0.9
TUR001	NAC	2018	47.40589	-117.52708	8	0.9
TUR002	NAC	2018	47.42308	-117.54186	9	1.0
TUR003	NAC	2018	47.43825	-117.53098	11	0.6
REV001	NAC	2018	47.07298	-117.93390	31	6.4
REV002	NAC	2018	47.07331	-117.93179	23	0.7
REV003	NAC	2018	47.07350	-117.93105	30	1.5
LAM001	NAC	2018	47.19631	-117.87850	22	0.3
GOO001	NAC	2018	46.93910	-119.27152	13	1.2
GOO002	NAC	2018	46.93417	-119.26875	17	0.9
GOO003	NAC	2018	46.93311	-119.26763	14	0.9
SEE001	NAC	2018	46.89602	-119.20178	11	0.7
SEE002	NAC	2018	46.91482	-119.20505	18	1.2
SEE003	NAC	2018	46.92900	-119.19260	11	0.9
CRA001	NAC	2018	46.83698	-119.75338	13	2.5
CRA002	NAC	2018	46.83824	-119.75217	7	0.9
CRA003	NAC	2018	46.83808	-119.75205	13	2.9
CRA004	NAC	2018	46.86905	-119.85042	16	0.9
CRA005	NAC	2018	46.87077	-119.84972	12	1.5
4*	NAC	2018	46.91275	-119.94497	18	1.2
QUI001	NAC	2018	47.21492	-119.98392	0	0.0
QUI002	NAC	2018	47.17855	-119.98058	0	0.0
QUI003	NAC	2018	47.16281	-119.98115	5	0.3
QUI004	NAC	2018	47.14401	-119.97972	10	0.8
QUI005	NAC	2018	47.15290	-119.97691	8	0.3
QUI006	NAC	2018	47.00597	-119.99372	17	0.7
QUI007	NAC	2018	47.06314	-120.00871	15	0.3
GP01	NAC	2015	46.23954	-121.97872	182	30.9

GP02	NAC	2015	46.27365	-121.96663	163	10.9
GP03	NAC	2015	46.32447	-121.99769	207	57.8
GP04	NAC	2015	46.30986	-122.05902	133	16.9
GP05	NAC	2015	46.33316	-121.97138	102	7.3
GP06	NAC	2015	46.24216	-121.61931	20	2.9
GP07	NAC	2015	46.27471	-121.60789	30	0.0
GP08	NAC	2015	46.27495	-121.60868	33	1.7
GP09	NAC	2015	46.28448	-121.64542	37	1.7
GP10	NAC	2015	46.29844	-121.68956	47	4.4
GP11	NAC	2015	46.29767	-121.71782	57	8.8
GP12	NAC	2015	46.32348	-121.72968	63	6.0
GP13	NAC	2015	46.35586	-121.72059	63	9.3
GP14	NAC	2015	46.36508	-121.72563	72	6.7
GP15	NAC	2015	46.37405	-121.72748	93	8.8
GP16	NAC	2015	46.39465	-121.73271	103	4.4
GP17	NAC	2015	46.42008	-121.75088	57	6.7
GP18	NAC	2015	46.43559	-121.76901	43	3.3
GP19	NAC	2015	46.44701	-121.79836	15	0.0
GP20	NAC	2015	46.45489	-121.86099	13	4.4
R01	NAC	2015	47.09090	-118.66449	32	3.0
R02	NAC	2015	47.09590	-118.62556	44	0.9
R03	NAC	2015	47.10487	-118.58917	39	1.2
R04	NAC	2015	47.10965	-118.55353	36	1.2
R05	NAC	2015	47.07618	-118.76224	34	1.2
R06	NAC	2015	47.07300	-118.80140	21	3.9
R07	NAC	2015	47.08041	-118.85823	31	1.7
UA 3165	MSB	2018	47.36531	-116.88715	30	NA
UA 3166	MSB	2018	47.06201	-116.84218	20	NA
UA 3167	MSB	2018	46.68531	-117.49476	5	NA
UA 3168	MSB	2018	46.72484	-117.01540	0.25	NA
UA 3169	MSB	2018	46.79586	-118.49359	10	NA
UA 3170	MSB	2018	46.39912	-120.25829	0	NA
UA 3172	MSB	2018	46.13610	-122.00622	20	NA
UA 3173	MSB	2018	46.27364	-121.96699	165	NA
UA 3180	MSB	2018	46.69403	-121.57717	5	NA
UA 3183	MSB	2018	46.92485	-119.99080	17	NA
UA 3184	MSB	2018	47.24977	-119.62904	11	NA
UA 3185	MSB	2018	47.66233	-117.92955	0	NA
UA 3186	MSB	2018	47.62130	-116.53016	7	NA
UA 3187	MSB	2018	47.47472	-115.87222	8	NA
UA 3188	MSB	2018	47.30643	-115.08864	0	NA
UA 3189	MSB	2018	47.06786	-114.07236	0	NA
DZ20_U02	USGS	1980	46.07314	-120.56090	0	NA
JD1	USGS	1980	46.40102	-117.93368	0	NA
JD21	USGS	1980	48.15350	-118.16926	0	NA
JD_U02	USGS	1980	48.22241	-118.70641	0	NA
SW230	USGS	1980	45.75209	-116.30656	0	NA
SW242	USGS	1980	45.93055	-116.13213	0	NA

SW264	USGS	1980	46.15249	-116.38834	0	NA
ZERO1	USGS*	1980	46.51557	-122.58064	0	NA
ZERO2	USGS*	1980	46.28927	-122.38057	0	NA
ZERO3	USGS*	1980	46.15799	-122.22019	0	NA
ZERO4	USGS*	1980	46.16969	-121.94199	0	NA
ZERO5	USGS*	1980	46.15473	-121.72912	0	NA
ZERO6	USGS*	1980	46.14391	-121.42943	0	NA
ZERO7	USGS*	1980	46.20645	-121.01211	0	NA
ZERO8	USGS*	1980	46.19882	-120.48630	0	NA
ZERO9	USGS*	1980	46.21223	-120.00160	0	NA
ZERO10	USGS*	1980	47.43408	-120.29860	0	NA
ZERO11	USGS*	1980	47.31251	-120.69668	0	NA
ZERO12	USGS*	1980	47.18999	-121.03930	0	NA
ZERO13	USGS*	1980	47.07555	-121.51592	0	NA
ZERO14	USGS*	1980	46.93412	-121.85886	0	NA
ZERO15	USGS*	1980	46.76922	-122.19835	0	NA
ZERO16	USGS*	1980	46.60746	-122.54435	0	NA
ZERO17	USGS*	1980	46.50250	-122.59753	0	NA
ZERO18	USGS*	1980	46.37848	-122.45773	0	NA
ZERO19	USGS*	1980	46.25248	-122.32189	0	NA
ZERO20	USGS*	1980	46.21122	-119.54898	0	NA
ZERO21	USGS*	1980	46.20459	-119.11273	0	NA
ZERO22	USGS*	1980	46.06434	-118.35202	0	NA
ZERO23	USGS*	1980	46.00278	-117.86435	0	NA
ZERO24	USGS*	1980	45.91521	-117.26884	0	NA
ZERO25	USGS*	1980	45.75386	-116.31184	0	NA
ZERO26	USGS*	1980	45.70491	-115.60763	0	NA
ZERO27	USGS*	1980	48.47602	-114.39371	0	NA
ZERO28	USGS*	1980	48.49176	-115.21806	0	NA
ZERO29	USGS*	1980	48.49741	-115.63047	0	NA
ZERO30	USGS*	1980	48.29764	-116.54271	0	NA
ZERO31	USGS*	1980	48.32150	-117.28466	0	NA
ZERO32	USGS*	1980	48.20839	-118.18046	0	NA
ZERO33	USGS*	1980	48.27079	-118.70632	0	NA
ZERO34	USGS*	1980	47.92290	-119.39868	0	NA
ZERO35	USGS*	1980	47.58697	-114.03059	0	NA
ZERO36	USGS*	1980	45.81134	-113.95606	0	NA
ZERO37	USGS*	1980	45.77819	-112.71924	0	NA
ZERO38	USGS*	1980	45.98599	-112.40231	0	NA
ZERO39	USGS*	1980	46.39735	-112.41281	0	NA
ZERO40	USGS*	1980	46.80866	-112.42355	0	NA
ZERO41	USGS*	1980	47.01431	-112.42900	0	NA
ZERO42	USGS*	1980	47.42560	-112.44010	0	NA
ZERO43	USGS*	1980	47.83685	-112.45144	0	NA
ZERO44	USGS*	1980	48.24806	-112.46305	0	NA
ZERO45	USGS*	1980	48.65925	-112.47491	0	NA
ZERO46	USGS*	1980	48.50472	-112.16091	0	NA
ZERO47	USGS*	1980	48.49343	-112.98580	0	NA

ZERO48	USGS*	1980	48.48741	-113.98189	0	NA

Table A.1: The thickness measurements used in the Layer Models. Samples in bold underwent geochemical analysis. Samples in bold underwent geochemical analysis. T= thickness; SE = ± 1 standard error; NAC = N. Cutler, MSB = M. Bolton. The detailed provenance of the measurements marked USGS* (i.e., zero measurements) is not clear from the original literature, but they are described in Durant et al. (2009) as originating from USGS documentation.

How does tephra deposit thickness change over time? A calibration exercise based on the 1980 Mount St Helens tephra deposit

Cutler, N.A.; Streeter, R.T., Engwell, S.L., Bolton, M.S., Jensen, B.J.L., Dugmore, A.J.

Author statement

Conceptualization: Nick Cutler & Britta Jensen
Methodology: Nick Cutler, Samantha Engwell & Britta Jensen
Formal analysis: Matthew Bolton, Nick Cutler & Samantha Engwell
Investigation: Matthew Bolton, Nick Cutler, Andrew Dugmore, Britta Jensen, Richard Streeter
Writing - Original Draft: Nick Cutler
Writing - Review & Editing: All authors
Visualization: Matthew Bolton & Nick Cutler
Supervision: Nick Cutler & Britta Jensen
Project administration: Nick Cutler
Funding acquisition: Nick Cutler

Declaration of interests

☒ The authors declare that they have no known competing financial interests or personal relationships that could have appeared to influence the work reported in this paper.

☐The authors declare the following financial interests/personal relationships which may be considered as potential competing interests:

The tephra layer produced by the 1980 eruption of Mount St Helens was surveyed;

Isopach maps derived from a) our survey & b) measurements made in 1980 were compared

Preservation of the tephra layer was good in undisturbed areas

Despite good preservation, our model overestimated the volume of the tephra deposit

Our results demonstrate the sensitivity of reconstructions to measurement location